University of Groningen

Port-Hamiltonian discretization for open channel flows

Pasumarthy, R.; Ambati, V.R.; Schaft, A.J. van der

IMPORTANT NOTE: You are advised to consult the publisher's version (publisher's PDF) if you wish to cite from it. Please check the document version below.

Document Version
Publisher's PDF, also known as Version of record

Link to publication in University of Groningen/UMCG research database
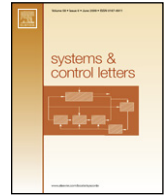
Port-Hamiltonian discretization for open channel flows

R. Pasumarthy [a,*], V.R. Ambati [b,*], A.J. van der Schaft [c]

[a] Department of Electrical Engineering, Indian Institute of Technology Madras, Chennai 600036, India
[b] Numerical Analysis and Computational Mechanics Group, Department of Applied Mathematics, University of Twente, 7500 AE, Enschede, The Netherlands
[c] Johann Bernoulli Institute for Mathematics and Computer Science, University of Groningen, P.O. Box 407, 9700 AK, Groningen, The Netherlands

ABSTRACT

A finite-dimensional Port-Hamiltonian formulation for the dynamics of smooth open channel flows is presented. A numerical scheme based on this formulation is developed for both the linear and nonlinear shallow water equations. The scheme is verified against exact solutions and has the advantage of conservation of mass and energy to the discrete level.

© 2012 Elsevier B.V. All rights reserved.

1. Introduction

Port based network modeling of complex lumped parameter physical systems naturally leads to a generalized Hamiltonian formulation of the dynamics. It results in a class of open dynamical systems called "Port-Hamiltonian" systems [1] that are defined using a power conserving interconnection structure called the Dirac structure, the Hamiltonian and dissipative elements. Such a generalized Hamiltonian formulation, called the "Port-Hamiltonian" formulation, has been successfully extended to classes of distributed parameter systems by introducing an infinite-dimensional Dirac structure based on Stokes' theorem. The key aspect of this formulation is that it allows a non-zero energy flow into the spatial domain through its boundary using the Dirac structure, whereas the standard Hamiltonian formulation assumes a zero energy flow through the boundary using the Poisson structure [2]. The Port-Hamiltonian formulation is also effectively used towards control design by using energy shaping methods. The technique relies on constructing a Lyapunov function by using the energy function of the system together with the conserved quantities called Casimirs [3].

The Port-Hamiltonian formulation [4] can be directly applied to model infinite-dimensional fluid dynamical systems containing all its physical conservation laws such as mass, momentum and energy (Hamiltonian). But for practical purposes, it is crucial to approximate these infinite-dimensional systems by a finite-dimensional system such that it is again a Port-Hamiltonian system cf., [5]. The finite-dimensional approximation then conserves most of the physical quantities of its infinite-dimensional counterpart and better captures the physics of the fluid dynamical system. To devise such a numerical scheme based on the finite-dimensional Port-Hamiltonian formulation, we choose a particular example of fluid flows, namely open channel flows. Preliminary works on such formulations are found in [6–8].

The one-dimensional shallow water equations governing open channel flows are the depth averaged approximations of the two-dimensional Navier–Stokes equations. They are a direct consequence of the conservation of mass and momentum and obey the conservation of energy for smooth flows but dissipate energy for non-smooth flows in the form of bores and hydraulic jumps. Many numerical methods exist for these equations such as finite volume methods [9,10] and discontinuous Galerkin finite element methods [11–13]. These numerical methods follow mass and momentum laws of balance, but they may not follow energy balance even in the smooth regions of a flow. Hence, we propose the use of the framework of Port-Hamiltonian systems which follows an energy balance law. Such a framework has implications towards the meteorological and oceanographic studies on geophysical flows, where the numerical schemes that conserve the energy are of great importance (for example following [14–16]).

A new numerical scheme based on a finite-dimensional Port-Hamiltonian formulation for the dynamics of shallow open

* Corresponding authors.
E-mail addresses: ramkrishna@ee.iitm.ac.in (R. Pasumarthy),
v.r.ambati@math.utwente.nl, vrambati@yahoo.co.in (V.R. Ambati),
a.j.van.der.schaft@rug.nl (A.J. van der Schaft).

channel water flow is the aim of the present paper. A shallow water channel with topography is first modeled as an infinite-dimensional Port-Hamiltonian system defined with respect to a Stokes–Dirac structure. Consequently, the system obeys a power conserving property, which is naturally equivalent to the energy balance, expressed in terms of power port variables called *flows* and *efforts* of the fluid dynamical system. For shallow water system, the *flows* are the rate of change of water depth and velocity, the *efforts* are the discharge and Bernoulli's function, and the shallow water equations are a direct consequence of the relation between flows and efforts captured by the Stokes–Dirac structure.

To model the shallow water canal as a finite-dimensional Port-Hamiltonian system, we tessellate the spatial domain with finite elements and approximate the flow variables with cell averages and effort variables with continuous piecewise linear polynomials. Such a choice of different approximation spaces for flows and efforts ensures the compatibility of the flow–effort relation in the Stokes–Dirac structure which are ordinary differential equations. Further, the continuity of efforts ensures the conservation of flow quantities. Consequently, each finite element will be a finite-dimensional Port-Hamiltonian system satisfying a power conserving property per finite element. We then enforce a discrete energy balance in the system by summing up the power conserving relation of all the finite elements. This effectively gives rise to an algebraic relation between the efforts and the corresponding discrete co-energy variables. Thus, the finite-dimensional Port-Hamiltonian system for a shallow water channel consists of a system of differential–algebraic equations.

The ordinary differential equations arising from the Port-Hamiltonian formulation are further discretized in time using an implicit mid-point time discretization. This time discretization is a second-order symplectic method and well-suited for a Hamiltonian system. After time discretization, the ODEs are transformed into nonlinear algebraic equations which are then solved by integrating them in pseudo-time using a five stage Runge–Kutta scheme until a steady state is reached in pseudo-time [11]. The numerical scheme is verified against several idealized exact solutions to show that it is first-order accurate and accurately conserves the energy.

2. Infinite-dimensional Port-Hamiltonian formulation

The Port-Hamiltonian formulation of fluid dynamical systems [4,17] is an extension of the Hamiltonian formulation incorporating non-zero flow through boundaries. Here, we present the Port-Hamiltonian formulation for open channel or canal water flows in one dimension.

2.1. Shallow water model

The dynamics of flow through an open channel of length L is governed by the shallow water equations which in one dimension read as

$$\partial_t h + \partial_x Q = 0 \quad \text{and} \quad \partial_t u + \partial_x B = 0 \quad \text{on } [0, L] \tag{1}$$

with $h(t, x)$ the water depth, $u(t, x)$ the depth averaged velocity, $Q = hu$ the flow discharge, $B = u^2/2 + g(h+b)$ the Bernoulli function and $b(x)$ the channel bed height measured from a fixed reference level. The shallow water equations (1) are completed together with the initial conditions $h(0, x) = h_0(x)$ and $u(0, x) = u_0(x)$, and inflow, outflow, solid wall or periodic boundary conditions at $x = 0$ and $x = L$. The total hydraulic energy (or Hamiltonian) in the open channel is

$$\mathcal{H} := \int_0^L \frac{1}{2} \left(hu^2 + g(h + b)^2 - gb^2 \right) \mathrm{d}x. \tag{2}$$

2.2. Preliminaries of differential geometry

The Port-Hamiltonian formulation is convenient in a differential geometric framework. For the one-dimensional shallow water model, we introduce the differential zero and one forms in one dimension. By definition, zero forms are functions that can be evaluated at any point on the domain and one forms are objects with a one-dimensional distribution that cannot be evaluated at a given point but can be integrated over any one-dimensional path of the domain. Now, the following operators relate zero and one forms in one dimension:

1. *Exterior derivative.* Consider a zero form or function $f(x) \in \mathbb{R}$ and a one form g defined as $g := (\partial f / \partial x) \mathrm{d}x$ which in coordinate-free language is given as $g = \mathrm{d}f$, where $\mathrm{d}(\cdot)$ is called the exterior derivative transforming the zero form to one form.
2. *Hodge star operator.* Consider a function $f(x) \in \mathbb{R}$ which by itself is a zero form and its one form $f \, \mathrm{d}x$. The Hodge star operator $*(\cdot)$ in one dimension is defined as $*f \, \mathrm{d}x := f$ and $*f := f \, \mathrm{d}x$ transforming a zero form to a one form and vice versa.
3. *Wedge product.* Given a zero form f and one form g, the wedge product $f \wedge g$ is defined as $f \wedge g := fg$ which is again a one form.

For more general definitions of these operators in n dimensions, we refer to [18]. Further, we denote the set of zero forms as $W^0(\Omega)$ and the set of one forms as $W^1(\Omega)$.

2.3. Stokes' Dirac structure

The Port-Hamiltonian formulation is based on the concept of a Dirac structure which is a geometric object formalizing the power conserving interconnections [1].

Definition 1. Let V be a linear space (possibly infinite-dimensional). There exists on $V \times V^*$ the canonically defined symmetric bilinear form

$$\langle\langle (f_1, e_1), (f_2, e_2) \rangle\rangle := \langle e_1 \mid f_2 \rangle + \langle e_2 \mid f_1 \rangle \tag{3}$$

with $f_i \in V$, $e_i \in V^*$, $i = 1, 2$ and $\langle \mid \rangle$ denoting the duality product between V and its dual subspace V^*. A constant Dirac structure on V is a linear subspace $D \subset V \times V^*$ such that

$$D = D^\perp, \tag{4}$$

where $\perp$ denotes the orthogonal complement with respect to the bilinear form $\langle\langle , \rangle\rangle$.

Let now $(f, e) \in D = D^\perp$. Then as an immediate consequence of (3),

$$0 = \langle\langle (f, e), (f, e) \rangle\rangle = 2\langle e \mid f \rangle.$$

Thus for all $(f, e) \in D$ we have $\langle e \mid f \rangle = 0$, expressing power conservation with respect to the dual power variables $f \in V$ and $e \in V^*$.

The Stokes–Dirac structure for the shallow water equations is defined as follows. The spatial domain $\Omega \subset \mathbb{R}$ is represented by a one-dimensional manifold with point boundaries. We associate the energy variables water depth $h(t, x)$ and velocity $u(t, x)$, with the one forms $h\mathrm{d}x \in V^1(\Omega)$, respectively $u\mathrm{d}x \in V^1(\Omega)$; and co-energy variables, Bernoulli function B and discharge Q, with zero forms as $(B, Q) \in V^0(\Omega)$ in which

$$V^1(\Omega) := W^1(\Omega) \times W^1(\Omega) \quad \text{and}$$
$$V^0(\Omega) := W^0(\Omega) \times W^0(\Omega) \tag{5}$$

where $W^0(\Omega)$ and $W^1(\Omega)$ are the space of zero and one forms, respectively. Now, the rate of energy variables, i.e., $f_h := -(\partial_t h)\mathrm{d}x$ and $f_u := -(\partial_t u)\mathrm{d}x$, are called *flows*; and the co-energy variables,

i.e., $e_h := \delta_h \mathcal{H} = B$ and $e_u := \delta_u \mathcal{H} = Q$, are called *efforts*. Furthermore, the values of the Bernoulli function B and the discharge Q evaluated at the boundaries would constitute the flow and effort variables at the boundary as $f_b = B|_{\partial\Omega} \in W^0(\partial\Omega)$ and $e_b = -Q|_{\partial\Omega} \in W^0(\partial\Omega)$ with $W^0(\partial\Omega)$ the space of zero forms on the boundary.

Consider the linear space of flow variables $\mathcal{F} = V^1(\Omega) \times W^0(\partial\Omega)$ and effort variables $\mathcal{E} = V^0(\Omega) \times W^0(\partial\Omega)$ together with the bilinear form

$$\left\langle\!\!\left\langle \left(f_h^1, f_u^1, f_b^1, e_h^1, e_u^1, e_b^1\right), \left(f_h^2, f_u^2, f_b^2, e_h^2, e_u^2, e_b^2\right)\right\rangle\!\!\right\rangle$$

$$:= \int_\Omega \left(e_h^1 \wedge f_h^2 + e_h^2 \wedge f_h^1 + e_u^1 \wedge f_u^2 + e_u^2 \wedge f_u^1\right)$$

$$+ \int_{\partial\Omega} \left(e_b^1 \wedge f_b^2 + e_b^2 \wedge f_b^1\right), \tag{6}$$

where $f_h := -(\partial h/\partial t)\,\mathrm{d}x, f_u := -(\partial u/\partial t)\,\mathrm{d}x, f_b := B|_{\partial\Omega}, e_h := B, e_u := Q, e_b := -Q|_{\partial\Omega}, (f_h^i, f_u^i, f_b^i) \in \mathcal{F}$ the flows, $(e_h^i, e_u^i, e_b^i) \in \mathcal{E}$ the efforts and $i = 1$ or 2. It has been shown in [4] that $\mathcal{D} \subset \mathcal{F} \times \mathcal{E}$ defined as

$$\mathcal{D} := \{(f, e) \in \mathcal{F} \times \mathcal{E} | f_h = \mathrm{d}e_u, f_u = \mathrm{d}e_h, f_b$$
$$= e_h|_{\partial\Omega}, e_b = -e_u|_{\partial\Omega}\} \tag{7}$$

is a Stokes–Dirac structure, i.e., $\mathcal{D} = \mathcal{D}^\perp$, with respect to the bilinear form $\langle\!\langle \cdot, \cdot \rangle\!\rangle$ defined in (6) and thus defines an infinite-dimensional Port-Hamiltonian system. The flow-effort relation in (7) is a direct consequence of the shallow water equations (1).

2.4. Power conserving property and energy balance

The Stokes–Dirac structure is always associated with a power conserving property stated as

$$\int_\Omega (e_h \wedge f_h + e_u \wedge f_u) + \int_{\partial\Omega} e_b \wedge f_b = 0. \tag{8}$$

Substituting the definitions of f_h, f_u, f_b, e_h, e_u and e_b in (8), we get

$$\int_\Omega \left(B\frac{\partial h}{\partial t} + Q\frac{\partial u}{\partial t}\right)\mathrm{d}x + \int_{\partial\Omega} BQ = 0. \tag{9}$$

Manipulating the first term in (9), the energy balance equation arises as follows

$$\frac{\mathrm{d}\mathcal{H}}{\mathrm{d}t} + (BQ)|_{x=L} - (BQ)|_{x=0} = 0. \tag{10}$$

3. Finite-dimensional Port-Hamiltonian formulation

A finite-dimensional Port-Hamiltonian formulation is obtained by approximating the flows and efforts such that they are compatible with the Stokes–Dirac structure and satisfy both the power conserving property and the energy balance equation.

3.1. Preliminaries

The flow domain $\Omega := [0, L]$ is tessellated with finite elements $K_k = [x_j, x_{j+1}]$, where x_j and x_{j+1} are the spatial coordinates of its nodes as shown in Fig. 1. On each finite element K_k, the one forms corresponding to the water depth and velocity field are approximated as

$$\hat{h}(t, x)\,\mathrm{d}x = \bar{h}_k(t)\,\psi \quad \text{and} \quad \hat{u}(t, x)\,\mathrm{d}x = \bar{u}_k(t)\,\psi; \tag{11}$$

where $\psi := \mathrm{d}x$ is the one form with $*\psi = 1$, $\bar{h}_k(t)$ is the mean water depth and $\bar{u}_k(t)$ is the mean velocity of the fluid in the finite element K_k. Subsequently, the approximation of flows is directly given as

$$\hat{f}_h(t, x) = -\partial_t \bar{h}_k\,\psi \quad \text{and} \quad \hat{f}_u(t, x) = -\partial_t \bar{u}_k\,\psi. \tag{12}$$

As a consequence, the flows are piecewise constant per finite element K_k and discontinuous across the nodes in the domain.

To satisfy the energy balance and mass conservation, the efforts $e_h = B$ and $e_u = Q$ are approximated with linear polynomials per element K_k such that they are continuous across each node. The approximation of efforts in each finite element K_k is therefore given as

$$\hat{e}_h = \hat{B}(t, x) = \hat{B}_j(t)\phi_j(x) + \hat{B}_{j+1}(t)\phi_{j+1}(x) \quad \text{and}$$

$$\hat{e}_u = \hat{Q}(t, x) = \hat{Q}_j(t)\phi_j(x) + \hat{Q}_{j+1}(t)\phi_{j+1}(x), \tag{13}$$

where $\phi_j(x) := (x_{j+1}-x)/(x_{j+1}-x_j)$ and $\phi_{j+1}(x) := (x-x_j)/(x_{j+1}-x_j)$ are shape functions, $\hat{B}_j(t)$ and $\hat{B}_{j+1}(t)$ are nodal values of the Bernoulli function B, and $\hat{Q}_j(t)$ and $\hat{Q}_{j+1}(t)$ are nodal values of the discharge Q. Finally, the approximation of boundary variables f_b and e_b on each boundary of the finite element K_k becomes

$$\hat{f}_b = \hat{e}_h|_{x=x_{j,j+1}} = \hat{B}_{j,j+1}(t) \quad \text{and}$$
$$\hat{e}_b = \hat{e}_u|_{x=x_{j,j+1}} = -\hat{Q}_{j,j+1}(t). \tag{14}$$

3.2. Discretization of the Stokes–Dirac structure

The discrete Port-Hamiltonian formulation starts by substituting the approximations of flows (12) and efforts (13) per finite element K_k in the flow–effort relations of the Stokes–Dirac structure (7) to get

$$-\partial_t \bar{h}_k \psi = \hat{Q}_j\,\mathrm{d}\phi_j + \hat{Q}_{j+1}\,\mathrm{d}\phi_{j+1} \quad \text{and}$$

$$-\partial_t \bar{u}_k \psi = \hat{B}_j\,\mathrm{d}\phi_j + \hat{B}_{j+1}\,\mathrm{d}\phi_{j+1}. \tag{15}$$

The choice of approximation of flows with piecewise constants and efforts with piecewise linear polynomial is made such that the flow–effort relation (15) is non-degenerate. Integrating (15) over the finite element K_k, the evolution of flows in terms of efforts per finite element emerge as

$$\frac{\mathrm{d}\bar{h}_k}{\mathrm{d}t} = \frac{1}{\Delta x_k}\left(\hat{Q}_j - \hat{Q}_{j+1}\right) \quad \text{and} \quad \frac{\mathrm{d}\bar{u}_k}{\mathrm{d}t} = \frac{1}{\Delta x_k}\left(\hat{B}_j - \hat{B}_{j+1}\right) \tag{16}$$

with $\Delta x_k = x_{j+1} - x_j$. The flow and effort approximations together with the boundary effort variables (14) automatically satisfy the power conserving property per finite element as follows

$$\int_{K_k} \left(\hat{e}_h \wedge \hat{f}_h + \hat{e}_u \wedge \hat{f}_u\right) + \int_{\partial K_k} \hat{e}_b \wedge \hat{f}_b$$

$$= -\frac{\Delta x_k}{2}\left(\hat{B}_{j+1} + \hat{B}_j\right)\frac{\mathrm{d}\bar{h}_k}{\mathrm{d}t} - \frac{\Delta x_k}{2}\left(\hat{Q}_{j+1} + \hat{Q}_j\right)$$

$$\times \frac{\mathrm{d}\bar{u}_k}{\mathrm{d}t} - \left(\hat{B}_{j+1}\hat{Q}_{j+1} - \hat{B}_j\hat{Q}_j\right) = 0. \tag{17}$$

The power conserving property (17) is deduced by using (12)–(14) in (8) and substituting (16). Having obtained a discretization for the Stokes–Dirac structure, it now remains to discretize the Hamiltonian and satisfy energy balance.

The Hamiltonian (or energy) is discretized in each finite element K_k as

$$\bar{\mathcal{H}}_k := \int_{K_k} \frac{1}{2}\left(\hat{h}\hat{u}^2 + g(\hat{h}+\hat{b})^2 - g\hat{b}^2\right)\mathrm{d}x$$

$$= \frac{\Delta x_k}{2}\left(\bar{h}_k\bar{u}_k^2/2 + g(\bar{h}_k+\bar{b}_k)^2 - g\bar{b}_k^2\right); \tag{18}$$

where $\hat{b}(x) := \bar{b}_k * \psi$ is the approximated bed height. The co-energy variables of the discretized Hamiltonian $\bar{\mathcal{H}}_k$ are then
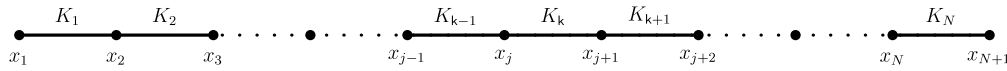
Fig. 1. Mesh stencil showing the numbering of elements and nodes with index k and j, respectively. Note that $j = k$ for $k = 1, \ldots, N$.

defined as

$$\bar{B}_k := \frac{\partial \bar{\mathcal{H}}_k}{\partial \bar{h}_k} = \left(\frac{1}{2} \bar{u}_k^2 + g(\bar{h}_k + \bar{b}_k) \right) \Delta x_k \quad \text{and}$$

$$\bar{Q}_k := \frac{\partial \bar{\mathcal{H}}_k}{\partial \bar{u}_k} = (\bar{h}_k \bar{u}_k) \Delta x_k. \tag{19}$$

We now enforce the following energy balance

$$\sum_{k=j=1}^{N} \left(\frac{\mathrm{d}\bar{\mathcal{H}}_k}{\mathrm{d}t} + \hat{B}_{j+1}\hat{Q}_{j+1} - \hat{B}_j\hat{Q}_j \right) = 0 \tag{20}$$

by equating the discretized effort variables to the co-energy variables at the interior nodes as

$$(\hat{B}_j, \ \hat{Q}_j) = (\alpha_j \bar{B}_{k-1} + \beta_j \bar{B}_k, \ \beta_j \bar{Q}_{k-1} + \alpha_j \bar{Q}_k)$$

$$\text{for } j = 2, \ldots, N; \tag{21}$$

and at the boundary nodes as

$$(\hat{B}_1, \ \hat{Q}_1) = (\bar{B}_1, \ \bar{Q}_0) \quad \text{and} \quad (\hat{B}_{N+1}, \ \hat{Q}_{N+1}) = (\bar{B}_N, \ \bar{Q}_L) \tag{22}$$

with $\alpha_j + \beta_j = 1$, $\alpha_j \in \mathbb{R}$ an arbitrary value for any $j = 2, \ldots, N$, $\bar{Q}_0$ and $\bar{Q}_L$ are the given inflow or outflow discharges at $x = 0$ and $x = L$, respectively. For a solid wall boundary, the inflow or outflow discharge is simply set to zero and for periodic boundaries, the boundary efforts are determined by making the two boundary nodes as a single interior node to obtain

$$\hat{B}_1 = \hat{B}_{N+1} = \alpha_1 \bar{B}_1 + \beta_1 \bar{B}_N \quad \text{and}$$

$$\hat{Q}_1 = \hat{Q}_{N+1} = \beta_1 \bar{Q}_1 + \alpha_1 \bar{Q}_N \tag{23}$$

with $\alpha_1 + \beta_1 = 1$ and α_1 an arbitrary value. The flow–effort relations (16) together with Eqs. (21)–(23) constitute the discretized dynamics of the shallow water equations.

Remark 1. To determine the efforts at each node j using (21), there exist several choices for α_j or β_j and can be arbitrarily chosen. In all the test cases, we made a simple choice of $\alpha_j = \beta_j = 1/2$.

3.3. Discrete conservation properties

Proposition 1. The Port-Hamiltonian discretization (16), (21) and (23) satisfy the mass and energy balance as follows

$$\frac{\mathrm{d}M}{\mathrm{d}t} + \hat{Q}_{N+1} - \hat{Q}_1 = 0 \quad \text{and} \quad \frac{\mathrm{d}E}{\mathrm{d}t} + \hat{B}_{N+1}\hat{Q}_{N+1} - \hat{B}_1\hat{Q}_1 = 0 \tag{24}$$

where $M := \sum_{k=1}^{N} \bar{h}_k \Delta x_k$ is the total mass and $E := \sum_{k=1}^{N} \bar{\mathcal{H}}_k$ the total energy.

Proof. The proof of mass balance is straightforward; evaluating the time derivative on total mass M using (16):

$$\frac{\mathrm{d}M}{\mathrm{d}t} = \sum_{k=1}^{N} \frac{\mathrm{d}\bar{h}_k}{\mathrm{d}t} \Delta x_k = \sum_{k=j=1}^{N} \left(\hat{Q}_j - \hat{Q}_{j+1} \right) = -(\hat{Q}_{N+1} - \hat{Q}_1). \tag{25}$$

To prove the energy balance, we first evaluate the time derivative on total energy E using (16) to find

$$\frac{\mathrm{d}E}{\mathrm{d}t} = \sum_{k=1}^{N} \frac{\mathrm{d}\bar{\mathcal{H}}_k}{\mathrm{d}t} = \sum_{k=1}^{N} \left(\bar{B}_k \frac{\mathrm{d}\bar{h}_k}{\mathrm{d}t} + \bar{Q}_k \frac{\mathrm{d}\bar{u}_k}{\mathrm{d}t} \right) \Delta x_k$$

$$= \sum_{k=j=1}^{N} \left(\bar{B}_k \left(\hat{Q}_j - \hat{Q}_{j+1} \right) + \bar{Q}_k \left(\hat{B}_j - \hat{B}_{j+1} \right) \right). \tag{26}$$

Rearranging the summation over elements in (26) into a summation over nodes and substituting the efforts determined in (21)–(23), we further find

$$\frac{\mathrm{d}E}{\mathrm{d}t} = (\bar{B}_1 \hat{Q}_1 + \bar{Q}_1 \hat{B}_1) - (\bar{B}_N \hat{Q}_{N+1} + \bar{Q}_N \hat{B}_{N+1})$$

$$+ \sum_{k=j=2}^{N} \left(\left(\bar{B}_k - \bar{B}_{k-1} \right) \hat{Q}_j + \left(\bar{Q}_k - \bar{Q}_{k-1} \right) \hat{B}_j \right)$$

$$= (\bar{B}_1 \bar{Q}_0 + \bar{Q}_1 \bar{B}_1) - (\bar{B}_N \bar{Q}_L + \bar{Q}_N \hat{B}_{N+1})$$

$$+ \sum_{k=2}^{N} \left(\bar{B}_k \bar{Q}_k - \bar{B}_{k-1} \bar{Q}_{k-1} \right)$$

$$= (\bar{B}_1 \bar{Q}_0 - \bar{B}_N \bar{Q}_L) = (\hat{B}_1 \hat{Q}_1 - \hat{B}_{N+1} \hat{Q}_{N+1}) \tag{27}$$

for a given inflow or outflow boundary conditions. For periodic and solid wall boundaries, we find that $\mathrm{d}E/\mathrm{d}t = 0$. □

3.4. Time discretization

The Port-Hamiltonian discretization (16) and (21)–(23) takes the following form:

$$\frac{\mathrm{d}\mathbf{y}}{\mathrm{d}t} = F(t, \mathbf{y}); \tag{28}$$

with $\mathbf{y} = (\bar{h}_1, \bar{u}_1, \ldots, \bar{h}_N, \bar{u}_N)^T$ the unknown flow variables and $F(t, \mathbf{y})$ the nonlinear right hand side obtained after substituting efforts (21)–(23) and co-energy variables (19) into the RHS of (16). To integrate the ordinary differential equations (28) in time, we employ an implicit mid-point time discretization to get

$$L(t^n, \mathbf{y}^n, t^{n-1}, \mathbf{y}^{n-1})$$

$$:= \mathbf{y}^n - \mathbf{y}^{n-1} - \Delta t \, F \left((t^n + t^{n-1})/2, (\mathbf{y}^n + \mathbf{y}^{n-1})/2 \right) = 0, \tag{29}$$

where $L(t^n, \mathbf{y}^n, t^{n-1}, \mathbf{y}^{n-1})$ represents the nonlinear algebraic equations. The implicit mid-point scheme is a second-order symplectic method [19] that is well-suited for Hamiltonian systems and leads to a stable numerical integration in time. The nonlinear equations (29) are solved by augmenting them with pseudo-time derivatives as

$$\Delta \mathbf{x} \cdot \frac{\mathrm{d}\mathbf{y}}{\mathrm{d}\tau} = \frac{-1}{\Delta t} L(t^n, \mathbf{y}, t^{n-1}, \mathbf{y}^{n-1}) \tag{30}$$

with $\Delta \mathbf{x} = (\Delta x_1, \Delta x_1, \ldots, \Delta x_N, \Delta x_N)^T$, $\Delta t = t^n - t^{n-1}$ the time step and integrating in pseudo-time using a five-stage Runge–Kutta integration scheme [11] until it reaches the steady state in pseudo-time. The five-stage Runge–Kutta scheme is

$$(1 + \alpha_s)\mathbf{y}^s = \mathbf{y}^0 + \alpha_s \lambda (\mathbf{y}^{s-1} - L(t^n, \mathbf{y}^{s-1}, t^{n-1}, \mathbf{y}^{n-1})); \tag{31}$$

where $s = 1$–5 are the Runge–Kutta stages, $\alpha_s = (0.0791451, 0.163551, 0.283663, 0.5, 1.0)$ the Runge–Kutta coefficients, and $\lambda = \Delta\tau/\Delta t$ and $\Delta\tau$ the local pseudo-time step. The time step $\Delta t = CFL_{\Delta t} \max \left(\Delta x_k/(|\bar{u}_k| + \sqrt{g\bar{h}_k}) \right)$ is chosen globally for all $k = 1, \ldots, N$, the pseudo-time step $\Delta\tau = CFL_{\Delta\tau} \Delta x_k/(|\bar{u}_k| + \sqrt{g\bar{h}_k})$ is chosen locally for each k, and $CFL_{\Delta t} = 1.0$ and $CFL_{\Delta\tau} = 0.9$ are the Courant–Friedrichs–Lewy (CFL) numbers for Δt and $\Delta\tau$, respectively.

4. Numerical examples

4.1. Burgers' equation

On a flat bed, the one-dimensional nonlinear shallow water equations take the form of Burgers' equation $\partial_t q + q \partial_x q = 0$, when one of its Riemann invariants is taken constant as $u + 2\sqrt{gh} = c$ with $q(x,t) = c - 3\sqrt{gh}$. An implicit exact solution is then constructed as

$$h(x,t) = (q(x,t) - c)^2/(9g) \quad \text{and}$$
$$u(x,t) = (c - 2q(x,t))/3 \tag{32}$$

with $q(x,t) = q_0(x')$ and $x = x' + q_0(x')t$, where $q(x,0) = q_0(x)$ is the initial condition. Now for any given initial condition $q_0(x)$ with $dq_0/dx < 0$ somewhere, wave breaking occurs at time $t_b = -1/\min(dq_0/dx)$.

We choose the initial condition as $q_0(x) = \sin(\pi x)$ with $x \in [0,2]$, $g = 1$, $c = 3$ and use periodic boundary conditions as given in (23). In our numerical simulation, this smooth initial condition develops into a discontinuity at time $t_b = 1/\pi$ as in the case of exact solution, see Fig. 2(a). Fig. 2(b) shows that the total discrete energy is conserved in time demonstrating the advantage of the Port-Hamiltonian based numerical scheme. We then compute the numerical errors in L^2 and L^∞ norms and the respective orders of accuracy for water depth h and velocity u at various instants of time on different mesh sizes, presented in Table 1. The order of accuracy in Table 1 clearly suggests that the numerical scheme is first-order accurate.

4.2. Flow over a bump

Analytical solutions for steady subcritical and supercritical flows over a given parabolic bump are given by Houghton and Kashara [20]. The parabolic bump is taken as

$$b(x) = \begin{cases} \dfrac{1}{2}\left(1 - \left(\dfrac{x-5}{2}\right)^2\right) & \text{if } |x-5| \le 2, \\ 0 & \text{if } |x-5| > 2 \end{cases} \tag{33}$$

in a channel from $x = 0$ to $x = 10$. The steady subcritical solution is obtained by solving the following equation for h and u at any $x = [0,10]$,

$$hu = Q_c \quad \text{and} \quad u^2/2 + g(h+b) = B_c \tag{34}$$

with $Q_c = 1$, $B_c = 25.5$ and $g = 25$ such that the Froude number $F = u/\sqrt{gh} < 1$. We initialize this steady exact solution in our numerical scheme and simulate until a steady state is numerically achieved with inflow $(\bar{h}_0, \bar{u}_0) = (\bar{h}_1, 1/\bar{h}_1)$ and outflow $(\bar{h}_L, \bar{u}_L) = (\bar{h}_N, \bar{u}_N)$ boundary conditions (see Fig. 3). At steady state, the errors and order of accuracy of water depth h and velocity u presented in Table 2 again shows that the scheme is first-order accurate.

4.3. Linear harmonic waves

The one-dimensional linear shallow water equations are

$$\partial_t \eta + \partial_x(Hu) = 0 \quad \text{and} \quad \partial_t u + \partial_x(g\eta) = 0, \quad x \in [0,L] \tag{35}$$

with η the free surface wave elevation measured from the water surface at rest, H the water depth at rest and $\mathcal{H} := \int_0^L (Hu^2 + g\eta^2)/2 dx$ the Hamiltonian. They satisfy a harmonic wave solution,

$$\eta(x,t) = A\sin(kx + \omega t), \quad \text{and}$$
$$u(x,t) = \left(\frac{-Agk}{\omega}\right)\sin(kx + \omega t) \tag{36}$$

with A the amplitude, $k = 2\pi m/L$ the wavenumber, ω the frequency, $T = 2\pi/\omega$ the time period, L the length of the domain, $\omega^2 = k^2 gH$ the dispersion relation, m any integer, and periodic boundary conditions. The Port-Hamiltonian scheme for linear shallow water equations is easily derived by treating h as η and defining $B := g\eta$ and $Q := Hu$.

We first initialized the exact solution (36) in the numerical scheme for linear shallow water equations setting $A = 0.01$, $L = 1$, $m = 1$, $g = 1$ and $H = 1$; and used periodic boundary conditions as given in (23). Linear harmonic waves are then simulated for 50 time periods on grids of size 20, 40, 80 and 160 elements with time step $\Delta t = T/32, T/64, T/128$ and $T/256$, respectively. Subsequently, we display the plots of free surface perturbation $\eta(t,x)$ at time $t = 50T$ and the discrete energy w.r.t. time in Fig. 4. It is clearly observed that the discrete energy is conserved and consequently there is no dissipation in the amplitude of the waves even after 50 time periods. However, the numerical scheme displays a dispersion error in the simulated waves which decreases from coarse to fine grids. Further, to show that the scheme is first-order accurate, we present numerical errors and orders of accuracy in Table 3 at various time instants.

Second, we initialized harmonic waves (36) in the Port-Hamiltonian scheme for nonlinear shallow water equations with $h(t,x) := H + \eta(t,x)$ and simulated until the smooth initial linear waves break because of the nonlinearity. The effects of nonlinearity are demonstrated by comparing the space–time evolution of harmonic waves using linear and nonlinear schemes in Fig. 5.

4.4. Standing waves

The one-dimensional linear shallow water equations (35) also satisfy a standing wave solution,

$$\eta(x,t) = A\cos(kx)\cos(\omega t) \quad \text{and}$$
$$u(x,t) = \left(\frac{Agk}{\omega}\right)\sin(kx)\sin(\omega t) \tag{37}$$

with solid wall boundary conditions at $x = 0$ and $x = L$. The standing wave solution (37) is initialized in the numerical scheme for linear shallow water equations setting $A = 0.01$, $L = 1$, $m = 1$, $g = 1$ and $H = 1$, and simulated by applying solid wall boundary conditions as $(\bar{h}_0, \bar{u}_0) = (\bar{h}_1, -\bar{u}_1)$ and $(\bar{h}_L, \bar{u}_L) = (\bar{h}_N, -\bar{u}_N)$. Comparison of the numerical solution of the standing wave against its exact solution after one time period and the discrete energy conservation in time is shown in Fig. 6(a) and (b). Numerical errors and the corresponding orders of accuracy tabulated in Table 4 infers that the scheme is first-order accurate.

4.5. Linearized wave maker

A linearized wave maker, applying a kinematic boundary condition $u(x = 0, t) = Agk\sin(kL)\cos(\omega t)/\omega$ at one end of a wave basin $x = 0$ and a solid wall boundary condition at the other end $x = L$, generates the following gravity wave field

$$\eta(x,t) = A\cos(k(L-x))\sin(\omega t) \quad \text{and}$$
$$u(x,t) = \left(\frac{Agk}{\omega}\right)\sin(k(L-x))\cos(\omega t) \tag{38}$$

satisfying the one-dimensional linear shallow water equations (35) with the dispersion relation $\omega^2 = gHk^2$ and $k = (2m+1)\pi/2$.

We initialize the exact solution (38) in our numerical scheme for the linear shallow water equations setting $A = 0.01$, $L = 1$, $m = 2$, $g = 1$ and $H = 1$; and numerically generate the waves by applying the time varying boundary conditions $(\bar{\eta}_0, \bar{u}_0) = (0, Agk\sin(kL)\cos(\omega t)/\omega)$ at the wave maker and solid

Table 1
Errors in L^2 and L^∞ norms for water depth h and velocity u of Burgers' solution at various time levels.

| Grid	Water depth (h)				Velocity (u)			
	L^2 error	Order	L^∞ error	Order	L^2 error	Order	L^∞ error	Order
	At $t = 0.09$							
20	6.3336e−02	–	1.1885e−01	–	6.2561e−02	–	1.1267e−01	–
40	3.1625e−02	1.00	5.9098e−02	1.01	3.1214e−02	1.00	5.6714e−02	0.99
80	1.5806e−02	1.00	2.9473e−02	1.00	1.5597e−02	1.00	2.8326e−02	1.00
160	7.9021e−03	1.00	1.4702e−02	1.00	7.7970e−03	1.00	1.4150e−02	1.00
	At $t = 0.18$							
20	7.1909e−02	–	1.9581e−01	–	7.1569e−02	–	1.8398e−01	–
40	3.5534e−02	1.02	9.8725e−02	0.99	3.5189e−02	1.02	9.6160e−02	0.94
80	1.7677e−02	1.01	4.8670e−02	1.02	1.7472e−02	1.01	4.7542e−02	1.02
160	8.8255e−03	1.00	2.4119e−02	1.01	8.7184e−03	1.00	2.3531e−02	1.01
	At $t = 0.27$							
20	9.2282e−02	–	3.1072e−01	–	9.2944e−02	–	2.8366e−01	–
40	4.9107e−02	0.91	2.2354e−01	0.48	4.9128e−02	0.92	2.1033e−01	0.43
80	2.4568e−02	1.00	1.3433e−01	0.73	2.4451e−02	1.01	1.3040e−01	0.69
160	1.2112e−02	1.02	6.9783e−02	0.94	1.2016e−02	1.02	6.9165e−02	0.91
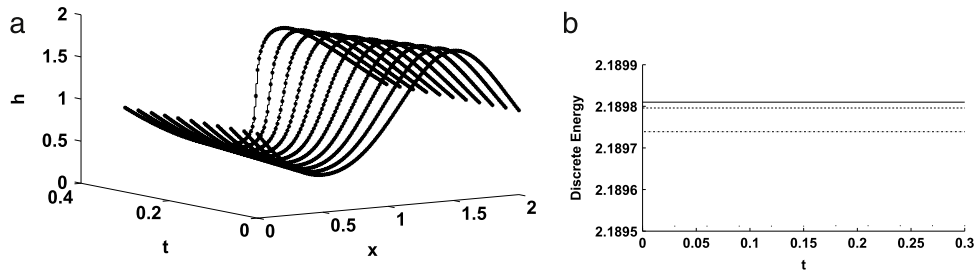
Fig. 2. Comparison of numerical solution of harmonic waves at $t = 6T$ using Port-Hamiltonian numerical scheme for linear (left) and nonlinear (right) shallow water equations on a grid of 80 elements. Observe the wave breaking phenomena due to nonlinearity. Exact and numerical solutions are marked with "$* - *$" and "$\circ - \circ$", respectively.
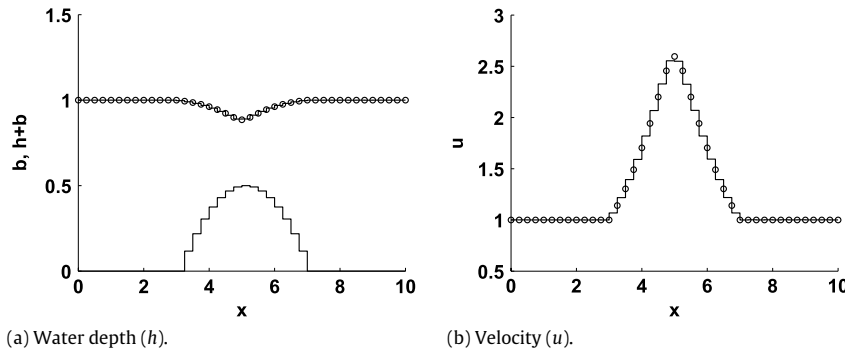

(a) Water depth (h).

(b) Velocity (u).

Fig. 3. Comparison of numerical solution ("–") of steady subcritical flow over bump against steady exact solution ("$\circ$") on a mesh stencil with 40 elements.

Table 2
Errors in L^2 and L^∞ norms for water depth h and velocity u of subcritical flow over bump at steady state.

Grid	Water depth (h)				Velocity (u)			
	L^2 error	Order	L^∞ error	Order	L^2 error	Order	L^∞ error	Order
20	9.5631e−02	–	9.1603e−02	–	2.3890e−01	–	2.0586e−01	–
40	4.7945e−02	1.00	4.8336e−02	0.92	1.1895e−01	1.01	1.0469e−01	0.98
80	2.3993e−02	1.00	2.4670e−02	0.97	5.9490e−02	1.00	5.1709e−02	1.02
160	1.1999e−02	1.00	1.2467e−02	0.98	2.9757e−02	1.00	2.5698e−02	1.01

wall boundary conditions $(\bar\eta_L, \bar u_L) = (\bar\eta_N, -\bar u_N)$ at the opposite end. The numerical simulations are carried out for 5 time periods on grids of size 20, 40, 80 and 160 elements with time step $\Delta t = T/16, T/32, T/64$ and $T/128$, respectively. In Table 5, the numerical errors and the corresponding orders of accuracy are tabulated.

We also simulate these waves in our nonlinear numerical scheme by initializing the exact solution in (38) with $h(t, x) =$

Table 3
Errors in L^2 and L^∞ norms for free surface perturbation and velocity of harmonic waves at various time levels.

| Grid	Free surface perturbation (η)				Velocity (u)			
	L^2 error	Order	L^∞ error	Order	L^2 error	Order	L^∞ error	Order
	At $t = 10T$							
20	3.355203e−03	–	5.741420e−03	–	3.139811e−03	–	5.526638e−03	–
40	8.750548e−04	1.94	1.755125e−03	1.71	8.682840e−04	1.85	1.746101e−03	1.66
80	2.589677e−04	1.76	5.914289e−04	1.57	2.587888e−04	1.75	5.912680e−04	1.56
160	9.494629e−05	1.45	2.240127e−04	1.40	9.494265e−05	1.45	2.240233e−04	1.40
	At $t = 30T$							
20	9.584440e−03	–	1.435877e−02	–	8.219201e−03	–	1.257490e−02	–
40	2.473886e−03	1.95	4.058127e−03	1.82	2.410303e−03	1.77	3.983402e−03	1.66
80	6.313784e−04	1.97	1.166671e−03	1.80	6.293884e−04	1.94	1.164016e−03	1.77
160	1.724456e−04	1.87	3.679616e−04	1.66	1.723894e−04	1.87	3.678919e−04	1.66
	At $t = 50T$							
20	1.355490e−02	–	1.962116e−02	–	1.203636e−02	–	1.751711e−02	–
40	4.096750e−03	1.73	6.331122e−03	1.63	3.926849e−03	1.62	6.122858e−03	1.52
80	1.030933e−03	1.99	1.741978e−03	1.86	1.025298e−03	1.94	1.735949e−03	1.82
160	2.668249e−04	1.95	5.119071e−04	1.77	2.666554e−04	1.94	5.116759e−04	1.76
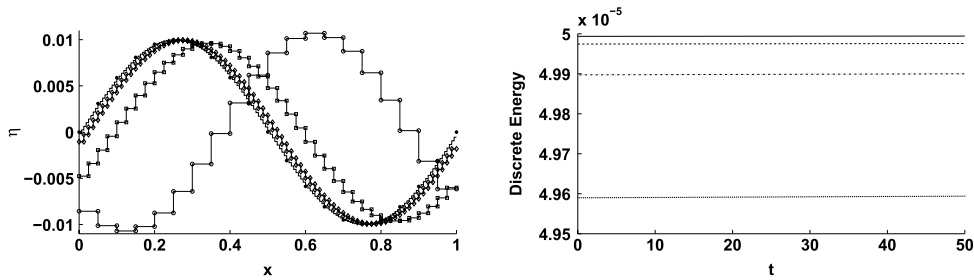
Fig. 4. *Left*: comparison of exact and numerical solution of free surface perturbation $\eta(t, x)$ at time $t = 50T$. Exact solution is marked with "∗" and numerical solution for 20 elements marked as "∘ − ∘", 40 elements as "□ − □", 80 elements as "◇ − ◇" and 160 elements as "−". *Right*: total discrete energy in the computational domain with a grid of 20 "..", 40 "-.-", 80 "- -" and 160 "−" elements.

(a) $t = 4T$. (b) $t = 4T$. (c) $t = 6T$.

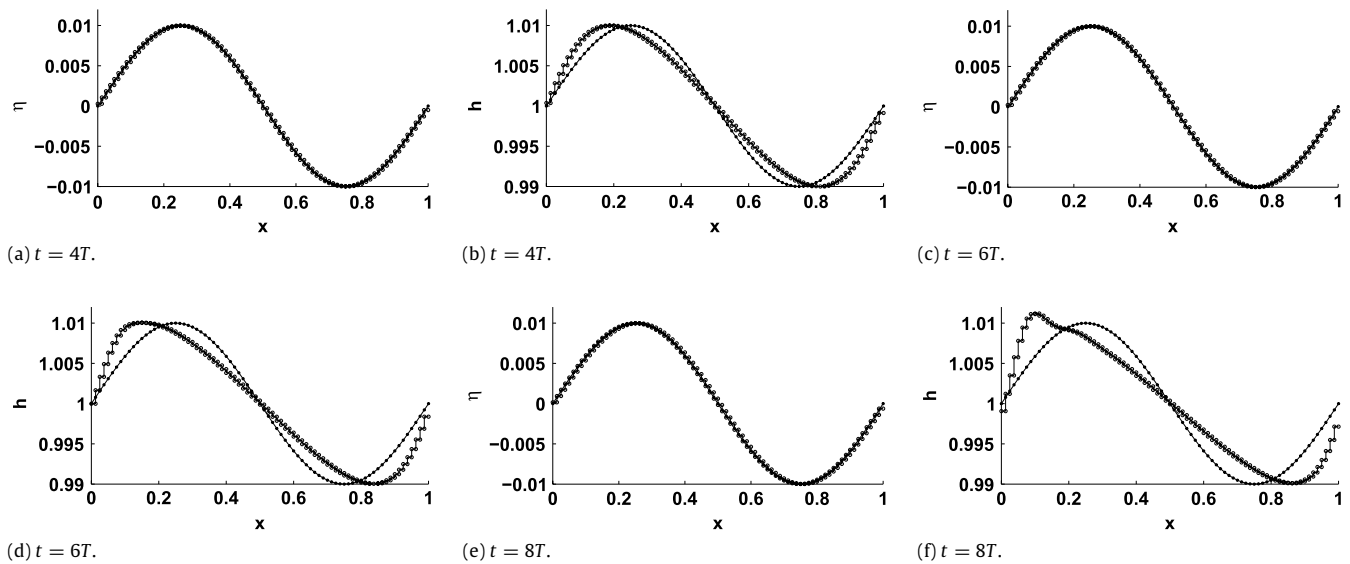(d) $t = 6T$. (e) $t = 8T$. (f) $t = 8T$.

Fig. 5. Numerical solution of harmonic waves using Port-Hamiltonian numerical scheme for linear (left) and nonlinear (right) shallow water equations on a grid of 80 elements. Exact and numerical solutions are marked as "∗ − ∗" and "∘ − ∘", respectively. Observe on the left, numerical harmonic waves are in good agreement with the exact solution and on the right side, the wave steepens due to nonlinearity.

$H + \eta(t, x)$ and applying the boundary conditions as $(\bar{h}_0, \bar{u}_0) = (\bar{h}_1, Agk \sin(kL) \cos(\omega t)/\omega)$ at the wave maker and $(\bar{h}_L, \bar{u}_L) = (\bar{h}_N, -\bar{u}_N)$. The evolution of the wave profile generated by the wave maker are compared against the exact solution at various time levels using both linear and nonlinear schemes are shown in Fig. 7. Both schemes capture the generated wave profiles and compare well with the exact solutions.

5. Conclusions

A finite-dimensional Port-Hamiltonian formulation for the nonlinear shallow water equations defined with respect to a Stokes–Dirac structure is presented. The key advantage of this formulation is that the physical properties of the infinite-dimensional model, such as mass and energy conservation, are

Table 4
Errors in L^2 and L^∞ norms for free surface perturbation and velocity of standing waves at various time levels.

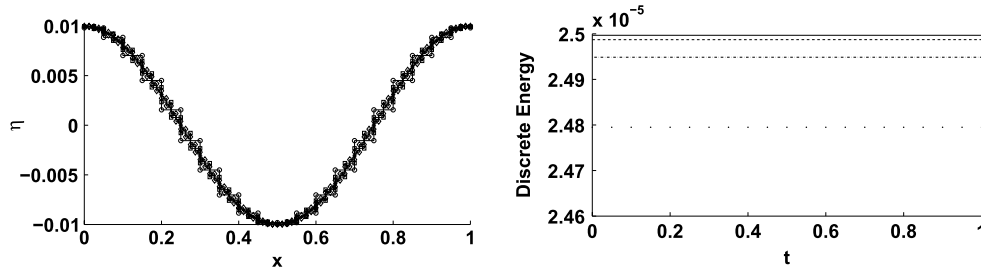| Grid	Free surface perturbation (η)				Velocity (u)			
	L^2 error	Order	L^∞ error	Order	L^2 error	Order	L^∞ error	Order
	At $t = T$							
20	6.4055e−04	–	1.1994e−03	–	5.3547e−04	–	7.5727e−04	–
40	3.2051e−04	1.00	6.0662e−04	0.98	1.3625e−04	1.97	1.9268e−04	1.97
80	1.6030e−04	1.00	3.0398e−04	1.00	3.4210e−05	1.99	4.8380e−05	1.99
160	8.0157e−05	1.00	1.5207e−04	1.00	8.5635e−06	2.00	1.2111e−05	2.00

Fig. 6. *Left*: comparison of exact and numerical solution of free surface perturbation $\eta(t, x)$ at time $t = T$. Exact solution is marked with "*" and numerical solution for 20 elements marked as "∘ − ∘", 40 elements as "□ − □", 80 elements as "⋄ − ⋄" and 160 elements as "−". *Right:* total discrete energy in the computational domain with a grid of 20 "..", 40 "-.-", 80 "- -" and 160 "−" elements.

Table 5
Errors in L^2 and L^∞ norms for free surface perturbation and velocity of linear waves generated by the wave maker at various time levels.

Grid	Free surface perturbation (η)				Velocity (u)			
	L^2 error	Order	L^∞ error	Order	L^2 error	Order	L^∞ error	Order
	At $t = 4.5T$							
20	6.9151e−03	–	1.1046e−02	–	1.7536e−03	–	4.3527e−03	–
40	3.4870e−03	0.99	5.2555e−03	1.07	9.8505e−04	0.83	2.3221e−03	0.91
80	1.7487e−03	1.00	2.5999e−03	1.02	4.9660e−04	0.99	1.1769e−03	0.98
160	8.7532e−04	1.00	1.2942e−03	1.01	2.4932e−04	0.99	5.9336e−04	0.99
	At $t = 5T$							
20	7.7623e−03	–	8.3400e−03	–	9.2686e−04	–	2.1405e−03	–
40	3.9154e−03	0.99	4.0551e−03	1.04	4.0376e−04	1.20	8.0402e−04	1.41
80	1.9620e−03	1.00	1.9938e−03	1.02	2.0052e−04	1.01	3.8678e−04	1.06
160	9.8155e−04	1.00	9.8971e−04	1.01	1.0020e−04	1.00	1.9164e−04	1.01

(a) $t = 3T/4$.

(b) $t = 3T/4$.

(c) $t = 7T/4$.

(d) $t = 7T/4$.
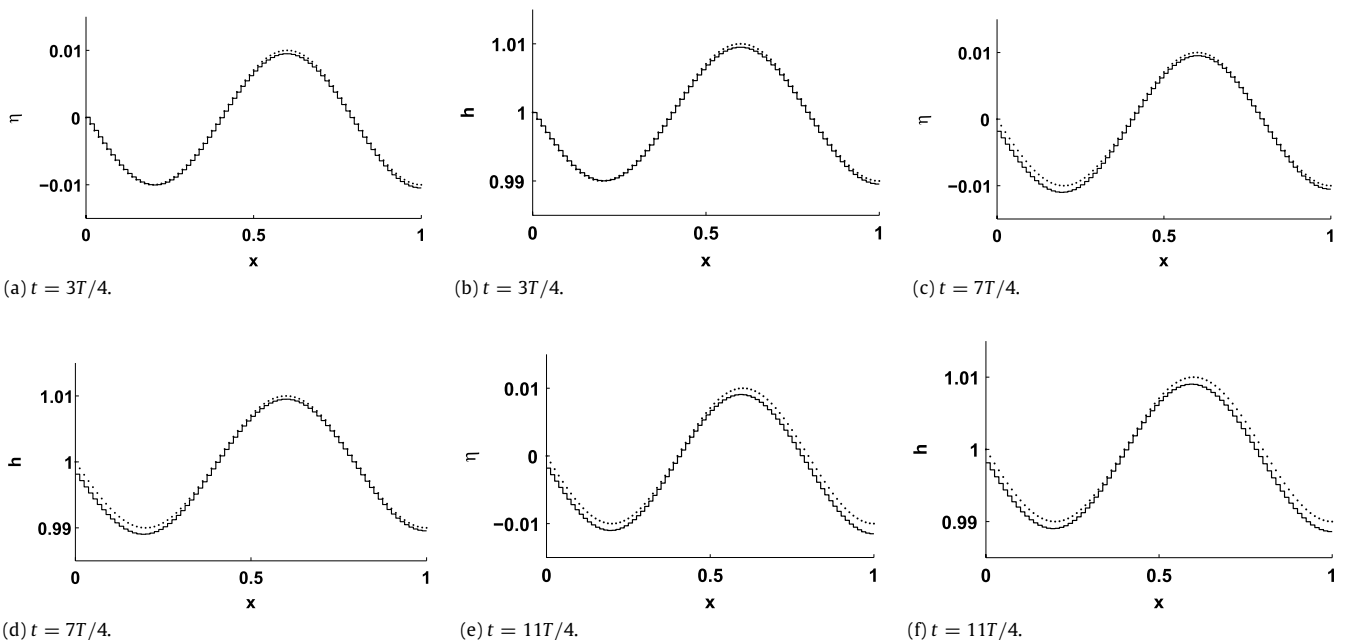
(e) $t = 11T/4$.

(f) $t = 11T/4$.

Fig. 7. Numerical solution of harmonic waves generated by a linear wave maker using Port-Hamiltonian numerical scheme for linear (left) and nonlinear (right) shallow water equations on a grid of 80 elements. Exact and numerical solutions are marked as "−" and "•", respectively. Observe that the numerically generated wave profiles are in good agreement with the exact solutions.

directly translated into the finite-dimensional model. Thus, the finite-dimensional model of shallow water equations preserves discrete mass and energy in time. It is useful to extend the present formulation to the shallow water equations in two dimensions and capture its important physical properties such as the conservation of potential vorticity and enstrophy that are of great interest in oceanographic and meteorological studies.

The Port-Hamiltonian based numerical scheme for the shallow water equations is developed and verified against exact solutions. It makes use of a symplectic time integration scheme stemming from implicit mid-point time discretization. This gave the advantage of preserving the discrete energy in time and resulted in a stable numerical scheme that is first-order accurate for the leading order approximation of flow variables in space. However, the scheme is valid only for smooth open channel flows as the underlying governing equations are in the primitive form. For non-smooth flows, the conservative form of shallow water equations is required as they satisfy the jump conditions at the bores or hydraulic jumps with the correct energy dissipating conditions. This was beyond the scope of our present work.

Acknowledgments

References

[1] A.J. van der Schaft, L_2-Gain and Passivity Techniques in Nonlinear Control, Springer-Verlag, London, 2000.
[2] P.J. Olver, Applications of Lie Groups to Differential Equations, second ed., Springer, Berlin, 1993.
[3] H. Rodriguez, A.J. van der Schaft, R. Ortega, On stabilization of nonlinear distributed parameter port-controlled Hamiltonian systems via energy shaping, in: Proceedings of the 40th IEEE Conference on Decision and Control, Orlando, FL, 2001.
[4] A.J. van der Schaft, B.M. Maschke, Hamiltonian formulation of distributed-parameter systems with boundary energy flow, J. Geom. Phys. 42 (2002) 166–194.
[5] G. Golo, V. Talasila, A.J. van der Schaft, B.M. Maschke, Hamiltonian discretization of boundary control systems, Automatica 40 (2004) 757–771.
[6] R. Pasumarthy, On analysis and control of interconnected finite and infinite-dimensional physical systems, Ph.D. Thesis, University of Twente, 2006.
[7] R. Pasumarthy, A.J. van der Schaft, A finite dimensional approximation of the shallow water equations: the Port-Hamiltonian approach, in: Proceedings of the 45th IEEE Conference on Decision and Control, San Diego, USA, 2006, pp. 3984–3989.
[8] R. Pasumarthy, A.J. van der Schaft, A Port-Hamiltonian approach to modeling and interconnections of canal systems, in: Proceedings of 16th International Symposium on Mathematical Theory of Networks and Systems, Kyoto, 2006, pp. 1436–1443.
[9] E. Audusse, F. Bouchut, M.-O. Bristeau, R. Klein, B. Perthame, A fast and stable well-balanced scheme with hydrostatic reconstruction for shallow water flows, SIAM J. Sci. Comput. 25 (6) (2004) 2050–2065.
[10] E. Audusse, M.-O. Bristeau, A well-balanced positivity preserving second order scheme for shallow water flows on unstructured meshes, J. Comput. Phys. 206 (2005) 311–333.
[11] V.R. Ambati, O. Bokhove, Space–time discontinuous Galerkin finite element for shallow water flows, J. Comput. Appl. Math. 204 (2) (2007) 452–462.
[12] V.R. Ambati, O. Bokhove, Space–time discontinuous Galerkin discretization of rotating shallow water equations, J. Comput. Phys. 225 (2) (2007) 1233–1261.
[13] P.A. Tassi, O. Bokhove, C.A. Vionnet, Space discontinuous Galerkin method for shallow water flows-kinetic and HLLC flux, and potential vorticity generation, Adv. Water Resour. 30 (4) (2007) 998–1015.
[14] O. Bokhove, M. Oliver, Parcel Eulerian–Lagrangian fluid dynamics for rotating geophysical flows, Proc. R. Soc. Lond. Ser. A 462 (2006) 2575–2592.
[15] J. Frank, S. Reich, The Hamiltonian particle mesh method for the spherical shallow water equations, Atmos. Sci. Lett. 5 (2004) 89–95.
[16] P.J. Morrison, Hamiltonian description of the ideal fluid, Rev. Mod. Phys. 70 (1998) 467–521.
[17] B.M. Maschke, A.J. van der Schaft, Port controlled Hamiltonian representation of distributed parameter systems, in: N.E. Leonard, R. Ortega (Eds.), Proceedings of IFAC Workshop on Lagrangian and Hamiltonian Methods for Nonlinear Control, Princeton University, 2000, pp. 28–38.
[18] R. Abraham, J.E. Marsden, T. Ratiu, Manifolds, Tensor Analysis, and Applications, Springer-Verlag, 1988.
[19] E. Hairer, C. Lubich, G. Wanner, Geometric Numerical Integration: Structure-Preserving Algorithms for Ordinary Differential Equations, second ed., in: Springer Series in Computational Mathematics, Springer-Verlag, Berlin, 2006.
[20] D.D. Houghton, A. Kasahara, Nonlinear shallow fluid flow over an isolated ridge, Comm. Pure Appl. Math. 21 (1968) 1–23.